International Journal of Mechanical, Industrial and Aerospace Sciences
ISSN: 2517-9950
Vol:10, No:4, 2016

# Simulations of Laminar Liquid Flows through Superhydrophobic Micro-Pipes

Mohamed E. Eleshaky

***Abstract*—**This paper investigates the dynamic behavior of laminar water flows inside superhydrophobic micro-pipes patterned with square micro-posts features under different operating conditions. It also investigates the effects of air fraction and Reynolds number on the frictional performance of these pipes. Rather than modeling the air-water interfaces of superhydrophobic as a flat inflexible surface, a transient, incompressible, three-dimensional, volume-of-fluid (VOF) methodology has been employed to continuously track the air–water interface shape inside micro-pipes. Also, the entrance effects on the flow field have been taken into consideration. The results revealed the strong dependency of the frictional performance on the air fractions and Reynolds number. The frictional resistance reduction becomes increasingly more significant at large air fractions and low Reynolds numbers. Increasing Reynolds number has an adverse effect on the frictional resistance reduction.

***Keywords*—**Drag reduction, laminar flow in micropipes, numerical simulation, superhyrophobic surfaces, microposts.

## I. Introduction

MICRO-FABRICATION technologies have been advanced to the extent that they can be easily utilized in the fabrication of microfluidic systems found inside electric cooling devices and artificial capillary vessel. The main advantage of these micro-fluidic systems is their low rate of fluid flow. However, for certain applications, decreasing their size results in increasing the surface to volume ratio of their micro-channels/micro-pipes which leads to substantial increase in the skin friction drag as well as the pressure gradient required to drive the fluid through these systems. Over the last sixteen years, researchers have focused on the development of a passive drag reduction technique [1] that uses superhydrophobic surfaces (SHS's) as a means to reduce skin-friction drag. These surfaces contain micro- or nano-scale features that could create air-liquid interfaces which reduce the contact area between the flowing liquid and the solid wall. In addition, the air retained within these features acts as a lubricant to the liquid flowing above it and hence, reduces the skin friction drag. According to the experimental study [2], up to 40% reduction in skin friction drag can be achieved under laminar flow condition using SHS's. However, the mechanism for this drag reduction still remains unclear, especially for flows through superhydrophobic micro-pipes. Recently, [3] and [4] investigated experimentally laminar flows through super-hydrophobic micro-tubes. Guan et al. [3] concluded that the drag reduction continuously enhances with the increase of Reynolds number and the improvement of the microcosmic structure on super-hydrophobic surfaces, whereas, [4] concluded that the drag reduction enhances up to a critical Reynolds number ($Re$ = 900) above which it remains almost the same.

Most of the theoretical studies focused on modeling of the flow in superhydrophobic micro-channels or micro-tubes (e.g., [5]-[9], to name a few) have assumed the existence of a Cassie state (state where air exists between features' cavities) despite a transition to a wetted Wenzel state (state where liquid fills the in-between features' cavities) could be the case. Additionally, they treated the air-liquid interface boundary as a shear-free/slip flat boundary with a pinning contact line. As pointed out by [10], depinning of the interface contact line may substantially affect the effective slip performance.

Most of the Computational fluid dynamics (CFD) studies focused on modeling of the flow in superhydrophobic microchannels or microtubes ([10]-[13], to name a few), have treated the inlet and outlet boundaries of the computational domain as periodic boundaries assuming fully developed flow. This practice does not account for the shape of the air layer at the inlet of the computational domain if it exists and, consequently, could lead to erroneous results. Also, this practice does not take into consideration the effects of inlet pressure on the shape of air-liquid interface. This inlet pressure varies according to the flow geometry (length and hydraulic diameter) and the mass flow rate (Reynolds number). Furthermore, most of the above CFD studies have used slip and no-slip boundary conditions to model the superhydrophobic surface considering the air-liquid interface shape as a flat and inflexible surface. According to [11] and [12], which utilized recently direct numerical simulation (DNS) to model micro-posts geometries applying flat inflexible slip and no-slip boundary conditions, this practice leads to the loss of flow details at the air-water interface. Teo and Khoo [13] showed numerically that, for flow through microtubes having transverse grooves, there is a critical interface protrusion angle for which the effective slip length becomes zero. In their study, the curvature of an interface with a pinning contact line was allowed to change depending on the pressure difference across the interface. Their predicted results indicate the importance of including the interface shape into the computations.

From the above literature review, it is evident that modeling the air-liquid interface of SHS's as an inflexible flat shape and assuming fully developed flow without taking into

Dr. Mohamed E. Eleshaky is an assistant professor with Public Authority for Applied Education & Training, College of Technological Studies, Department of Mechanical Engineering Technology, P.O. Box 43418, Hawally 32049, Kuwait (phone: +96599545962; fax: +965-2532-0460; esheky@aim.com)

consideration the entrance region could lead to erroneous results. In addition, it is noticed that most of the previous studies focused on micro-channels and only few have focused on micro-pipes with transverse grooves patterned SHS's. Also, taking into consideration the flow operating conditions (inlet mass flow rate and outlet pressure), rather than assuming a fully developed flow, has not been addressed computationally by anyone other than Eleshaky [14] who recently used a VOF methodology for continuous tracking of the air–water interface shape inside micro-pipes rather than modeling the interfaces as a flat inflexible surface. He investigated water laminar flows through superhydrophobic micro-pipes patterned with micro-ridges features and micro-posts features. The dynamic behavior of these flows was not thoroughly investigated, especially, for the case of square micro-posts features. Therefore, the objectives of the present study are: (1) To investigate the dynamic behavior of laminar water flows inside superhydrophobic micro-pipes having square micro-posts features under different operating conditions; and (2) To study the effects of air fraction and Reynolds number on the frictional performance of these pipes.

## II. Numerical Modeling

### A. Governing Equations

In this study, the governing equations are the incompressible unsteady Navier-Stokes equations for three-dimensional laminar flow. Their indicial notation form in Cartesian coordinates is given by:

$$\frac{\partial \rho}{\partial t}+\frac{\partial(\rho u_i)}{\partial x_i}=0 \tag{1}$$

$$\frac{\partial(\rho u_i)}{\partial t}+\frac{\partial(\rho u_i u_j)}{\partial x_j}=-\frac{\partial \overline{P}}{\partial x_i} + \frac{\partial}{\partial x_j}\left[\mu\left(\frac{\partial u_i}{\partial x_j}+\frac{\partial u_j}{\partial x_i}-\frac{2}{3}\delta_{ij}\frac{\partial u_l}{x_l}\right)\right]+\rho g_i + F_{\sigma_i} \tag{2}$$

In (1) and (2), $\rho$ is the density, $t$ is the time, $\mu$ is the dynamic viscosity, $g_i$ is the gravity component in the $i$-direction, and $F_{\sigma i}$ is the $i$-component of the body force due to the surface tension. The values of $i$ and $j$ could be 1, 2, or 3 to represent properties in $x$, $y$, or $z$ directions, respectively. For example, $u_1$ is the component of the Cartesian velocity component, $u$, in the $x$-direction. $\delta_{ij}$ is Kronecker delta symbol which is equal to unity when $i = j$ and zero when $i \neq j$.

To continuously track the air-water interface, a volume of fluid (VOF) methodology [15] is used. This methodology first solves (1) and (2) for each phase (air or water) and then solves a scalar equation to obtain a quantity called the volume fraction, $\alpha$. This scalar quantity is defined as the percentage of water phase volume contained inside the computational cell relative to the cell total volume. Hence, $\alpha$ is equal to zero when the cell is filled only with air and is equal to one when it is filled only with water. If the value of $\alpha$ is between 0 and 1, the computational cell is considered an "interface" cell between the two phases. The equation governing the volume fraction, $\alpha$, is given by the following indicial notation form in Cartesian coordinates:

$$\frac{\partial \alpha}{\partial t}+\frac{\partial(\alpha u_i)}{\partial x_i}=0 \tag{3}$$

Knowing the volume fraction value of the computational cell, the fluid properties are updated by using:

$$\mu=\alpha\mu_w+(1-\alpha)\mu_a \tag{4}$$

$$\rho=\alpha\rho_w+(1-\alpha)\rho_a \tag{5}$$

where $\mu_a$ and $\mu_w$ are the air and water viscosities, respectively. $\rho_a$ and $\rho_w$ are the air and water densities, respectively.

In this study, the CSF model of [16] given by the following relation is used to approximate the surface tension term, $F_{\sigma_i}$, in the momentum equation (2):

$$F_{\sigma_i}=\sigma\frac{\rho\kappa}{\frac{1}{2}(\rho_w+\rho_a)}\frac{\partial \alpha}{\partial x_i} \tag{6}$$

where $\sigma$ is the air/liquid interfacial tension force and in the present study it takes the value of 0.072 N/m, $\rho$ is the discontinuous density. The "κ" term is the interface curvature given by:

$$\kappa=\nabla\cdot\hat{n} \tag{7}$$

where $\hat{n}$ is the unit normal to the interface surface and is given by:

$$\hat{n}=\frac{\nabla\alpha}{|\nabla\alpha|} \tag{8}$$

### B. Computational Grid

In this study, the micro-pipe configuration shown in Fig. 1 is analysed. The micro-pipe contains SHS's patterned with regularly arranged in-phase square micro-posts of similar sizes. The posts width, height, and transverse/longitudinal spacing are $w_{post}$, $H$, and s, respectively, as illustrated in Fig. 1. The air fraction, $AF$, is defined as $[1 - (w_{post} / (w_{post} + s))^2]$. The internal diameter of the micro-pipe ($D$) after adding the superhydrophobic features is equal to 152.34 μm and it is found that a pipe length of 3600 $\mu$m is sufficient to reach a fully developed flow for the considered flow cases. The post height, $H$, is 45 $\mu$m and is kept the same for all the considered cases herein. Also, for all the studied cases, the flow problem is assumed to be symmetrical about $x$-$z$ and $y$-$z$ planes, hence, only one quarter of the micro-pipe along the axial flow direction is considered in the computations. Fig. 2 shows part of the three-dimensional grid used in the computations. Here, $z$ is pointing in the downstream axial flow direction, while, $x$

and *y* are increasing in the outward radial direction following a right-handed Cartesian coordinate system. The computational domain extends 3600 $\mu$m in the downstream axial direction and 121.34 $\mu$m in the other two directions. Hybrid hexahedral/ tetrahedral control volumes are used to discretize the pipe domain. Based on grid independency tests, 1,723,320 hexahedral/ tetrahedral grid cells were found to produce an acceptable accuracy. These tests resulted in a minimum cell size of 1.012 $\mu m^3$ in the region of high gradients.

### C. Boundary Conditions

Referring to Fig. 2, different conditions are specified explicitly on the boundaries of the computational domain. At the inlet plane (*bc* 1), a value of zero is set for the air mass flow rate and a none-zero is prescribed for the water mass flow rate depending on the required Reynolds number $\left(\dot{m} = \frac{A\mu \mathrm{Re}}{D_h}\right)$, where *A* is the flow cross sectional area, *Re* is the Reynolds number, and $D_h$ is the hydraulic diameter. The normal of the inlet plane is prescribed for the velocity direction, whereas, the velocity components (*u, v, w*) and the pressure are calculated numerically. This practice is realistic as it permits the flow velocities to evolve naturally. At the outlet plane *(bc* 2*)*, the atmospheric pressure is prescribed for the pressure, *P*, and the normal gradients of all other variables (*u, v, w,* and $\alpha$) are set to zero. On the hydrophobic surfaces (*bc* 3), no-slip conditions and a contact angle of 128° are prescribed. At the *x–z* plane (*bc* 4), symmetry conditions are prescribed where the normal velocity component ($u_2$) is set to zero and the normal gradients for other variables are set to zero. At the *y–z* plane (*bc* 5), the normal velocity component ($u_1$) is set to zero and the normal gradients for other variables are set to zero.

### D. Initial Conditions

The micro-pipe configuration except the inlet plane is assumed to be filled initially with air. Whereas, the inlet plane is assumed to be all the time filled completely with water. This means that the initial air-liquid interface is in the form of a circular cross section. The VOF model is used to track the interface as the water flows inside the micro-pipe.

### E. Numerical Solver

In this study, the computational fluid dynamics (CFD) flow simulation package designated ANSYS FLUENT® V13.1 [17] is adopted to solve the governing equations using finite volume method. The pressure and convective terms in this method are second-order upwind differenced, whereas, the viscous terms are centrally differenced. A second-order implicit approach is used for time discretization and the calculation time-step is kept at 0.5 $\mu$s for all simulations. In the present study, the adopted VOF methodology uses a compressive interface capturing discretization scheme [18] to achieve a sharp interface. Due to the non-linearity of the governing equations, about 40 iterations are required per each time step to obtain a converged solution of $10^{-5}$ set as a criterion for the convergence of the flow equations and volume fraction equation. For the preformed simulations, an average of 4200 time-steps is required for the water flow to reach the end of micro-pipe. The computational time for these 4200 time-steps is about 180 hrs on a PC having an Intel® Core™ i7-4910MQ Processor and 32 GB of memory.

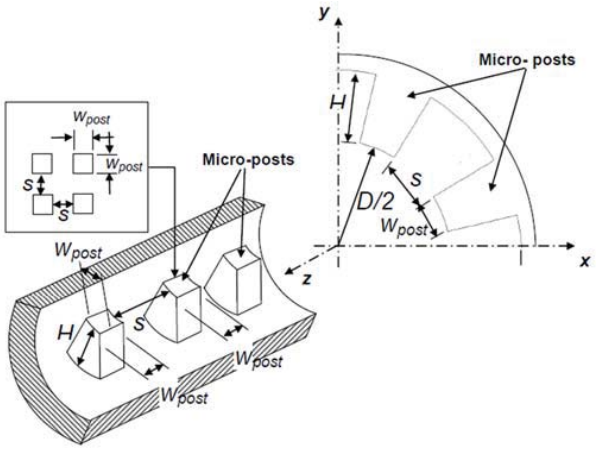


Fig. 1 Geometric structure of the superhydrophobic micro-pipe wall with square micro-posts size (side $w_{post}$ and height *H*) and transverse/longitudinal spacing *s*

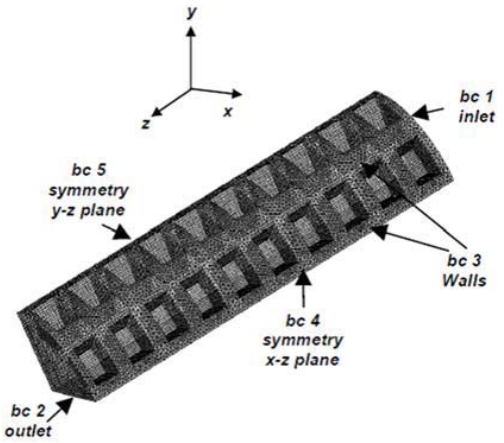


Fig. 2 Computational grid for micro-pipe with square micro-posts features

## III. Results and Discussions

### A. Comparisons with Previously Published Data

For methodology validation purposes, a numerical simulation is carried out for a case where water flows inside a channel patterned with micro-ridges features (Fig. 3) under laminar conditions. This case has previously been investigated by [19] using a Micro-*PIV* experimental technique.

The measured velocity profiles above the air-water interfaces are compared with their corresponding computational ones in Figs. 3 (b) and (c). It is obvious that the predicted and measured velocity profiles compare fairly well and a velocity slip of more than 0.15 $U_{max}$ exists on the air–water interface. This demonstrates the capability of the present

VOF methodology in handling the laminar flow inside confined micro-conduits.

*B. Flow Dynamics in Superhydrophobic Micro-Pipes*

A major characteristic of the superhydrophobic surfaces is the production of an air layer under the flowing liquid which acts as a lubricant to the liquid. The numerical solutions obtained in the present study provide an opportunity for detailed examination of the shape of the air-liquid interface between the square posts, hence, provide an insight into the dynamics of the flow in micro-pipes with SHS's. In order to visualize the shape of the air-liquid interface along the micro-pipe, the water volume fraction for the case of 0.6 air fraction and a mass flow rate of $4.786 \times 10^{-05}$ kg/s ($Re$ = 400) is plotted at different flow times on a 22.5°-plane passing through the square posts all the way till the end of the micro-pipe (Fig. 4). It is obvious that, at all flow times, the inlet flow region exhibits a Wenzel state. As the water proceeds along the micro-pipe, a Cassie state starts to form while the size of the Wenzel state region does not change. After the water reaches the end of the micro-pipe, the air-water interface shape remains the same and an air cushion is formed under the water leading to the obtained reduction in the drop of total pressure and, consequently, the skin-friction drag. As can be noticed from this figure most of the micro-pipe length is in the Cassie state.

*C. Influence of Air Fraction AF*

The main purpose of using superhydrophobic surfaces in micro-pipes is to reduce liquid-solid contact area, thereby reducing the frictional resistance between the liquid and the micro-pipe wall surface. As some of the solid surface on the micro-pipe wall is removed and replaced with arrays of air, the frictional resistance at the micro-pipe surface can significantly decrease due to reduced friction between the liquid and the air.

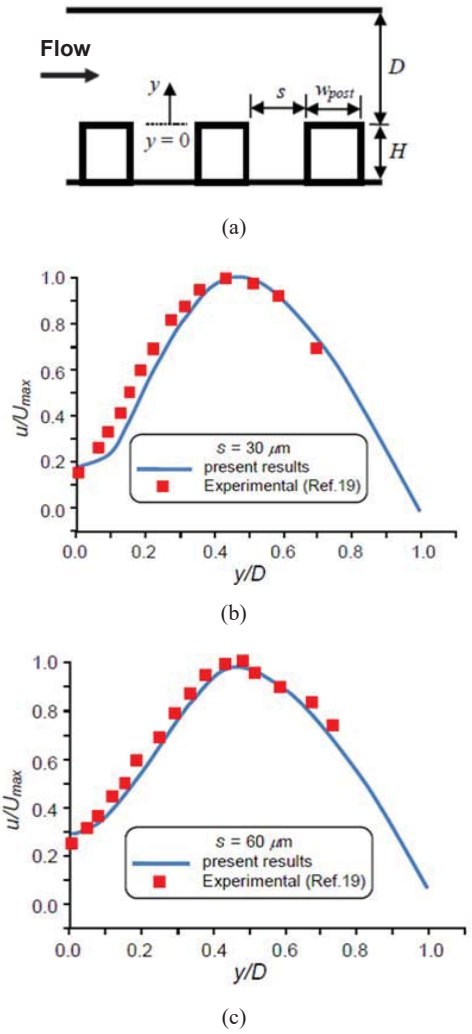


Fig. 3 Verification using a micro-channel with patterned surface; (a) Channel configuration, $w_{post}$ = 30 μm, $H$ = 20 μm, and $D$ = 200 μm; (b) and (c) Velocity profiles for $s$ = 30 μm and 60 μm, respectively

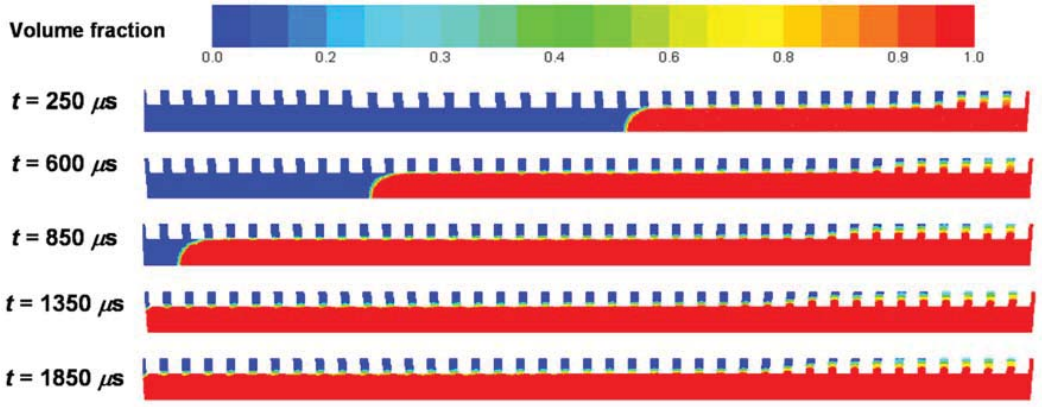


Fig. 4 Contours of water volume fraction as the water flows through superhydrophobic micro-pipe patterned with square posts. ($AF$ = 0.6 and $Re$ = 400

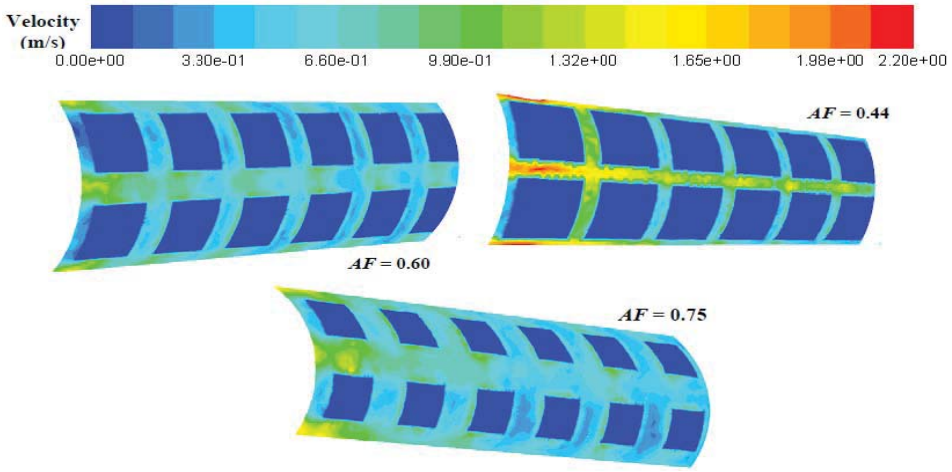


Fig. 5 Contours of velocity magnitude on a plane passing over the post-top faces at the micro-pipe end region for different air fractions (*Re* = 400)

In order to examine and quantify (characterize) the relationship between the air fraction and the frictional resistance reduction, it is helpful to first observe, discuss, and compare the velocity contours at a cylindrical plane passing over the surface of the posts at different air fractions, where all other parameters and flow conditions are exactly similar. Fig. 5 shows contours for *AF* = 0.44, 0.60, and 0.75, and *Re* = 400. As can be seen, all velocity contours are quite similar and the velocity is high over the cavity regions where slip condition exists. For all air fractions, the velocity is greatest in the region of the cavity mid-span. Near the surface of the post, the velocity tends to slow down due to high shear stress and the no-slip condition at the liquid-solid interface. In order to satisfy the conservation of mass principle and from the microscopic point of view, the liquid within the considered computational domain must speed up locally in the cavity regions between the posts, due to the deceleration over the solid post surfaces. Therefore, it is evident that the reduction in liquid-solid contact area is responsible for this increase in liquid momentum over the cavity regions. The non-zero velocity at these planes over the cavity regions is the slip velocity. The overall effect of this slip from the macroscopic viewpoint is an apparent or net slip velocity over the entire superhydrophobic wall. The surface area-weighted average slip velocity for *AF*= 0.44, 0.6, and 0.75 are about 17.5%, 25.3%, and 28.8 %, respectively, of the average liquid velocity through the micro-pipe. Hence, one can conclude that there is a direct relationship between the air fraction and the slip velocity, *i.e*., as air fraction is increased the apparent slip velocity is also increased. A direct result of the apparent slip velocity is an overall decrease in the total pressure drop of the liquid flow through the micro-pipe, for a specified volume flow rate.

Considering the overall surface geometry and its effect on the liquid flow through the micro-pipe, it is useful to mention that the arrays of posts create a checkerboard type surface as illustrated in Fig. 5. As a result, there tends to be a series of cavity "canals" parallel, and cavity regions transverse, to the flow. The absence of any solid surface along the cavity canals resembles the cavity regions that exist in longitudinal micro-rib patterned surfaces. Conversely, the presence of the posts creates cavity regions between successive posts in the stream-wise direction that should be similar in their effect to the cavity regions that exist in transverse micro-ribs patterned surfaces. It is important to redirect one's attention to Fig. 5 to note that the high velocity regions occur within the longitudinal cavity canals, and lower velocities occur inside the transverse cavity regions. As the liquid flows over an array of posts, it encounters a periodic series of slip and no-slip flow conditions, however, the liquid glides over a cushion of air as it flows above the longitudinal cavity canals. Therefore, it would seem logical to conclude that superhydrophobic surfaces with micro-posts should perform somewhere between surfaces that exhibit parallel and transverse micro-ribs.

Velocity contours near the edges of the post in Fig. 5 indicate large changes in the velocity as the liquid approaches the solid surface of the post. It is along the edges and at the corners that the velocity gradients are highest compared with other parts of the micro-pipes. These increased velocity gradients result from the high shear stress that prevails along the surface of the posts.

Average shear stress contours on the same cylindrical plane which passes through the post-top faces are illustrated in Fig. 6 for different air fractions and *Re* = 400. As can be seen, the shear stress over the entire cavity region is zero. The patterns on these shear stress contours are similar; near the edges, and especially near the corners, much higher shear stress than at other regions of the post exists due to the elevated velocity gradients in these regions. For these air fractions, there are some significant differences that are useful to mention. The maximum shear stress region for *AF* = 0.44 has an average value of 293 Pa, whereas the maximum for the case of *AF* = 0.75 is 978 Pa. The 70.5% increase in the air fraction amounts to a substantial increase of 236.8% in the maximum shear stress over the solid micro-post surface. This result is expected, since by decreasing the liquid-solid contact area

while keeping all other parameters such as *Re* constant, smaller solid surface will be subjected to the same shear fluid inertia due to the flowing liquid. The natural result is a rise in the micro-post surface shear stress. Because of the tremendous rise in shear stress on the post surface as the air fraction is increased, real-life application of such superhydrophobic surfaces could be challenging. In the ideal situation, the durability of the micro-posts is important since any fracture or damage of the posts could make the surface more susceptible to wetting. Hence, altering the shape of the posts by eliminating or reducing sharp edges and corners could potentially reduce the surface shear stress and overall surface friction even further. Rounding the sharp corners or even considering cylindrical posts with the same surface area as the square posts would be an interesting exploratory topic for further studies.

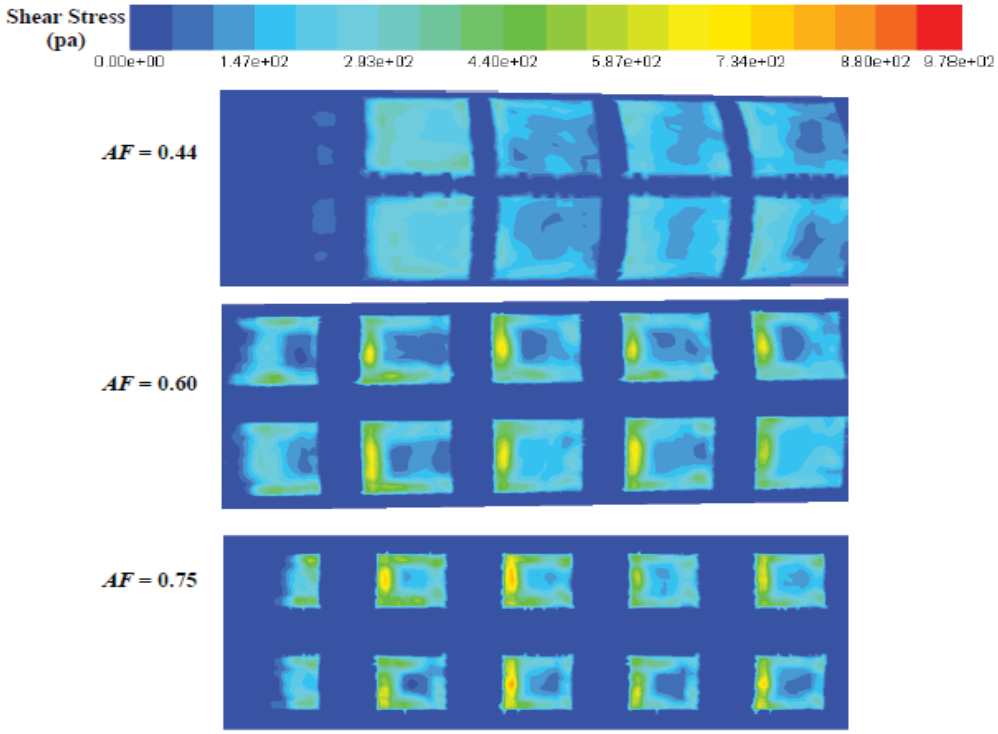


Fig. 6 Contours of wall shear stress on a plane passing over the post-top faces at the micro-pipe end region for different air fractions. (*Re* = 400)

The overall influence of cavity fraction on the local slip velocity is also investigated by considering the line plots of normalized velocity ($V/V_{avg\_ns}$) along a line passing through the mid-cavity and mid post-top faces. This line lies on the cylindrical plane which passes through all post-top faces ($R = D/2$). These results are illustrated in Fig. 7 (a) for air fractions of $AF$ = 0.44, 0.60, and 0.75 and $Re$ = 400. $V/V_{avg\_ns}$ is shown as a function of $z/(w_{post}+ s)$, where $z$ is in the flow direction and $(w_{post}+ s)$ is the total post/cavity width. $z/(w_{post}+ s) = 0$ corresponds to the trailing edge of a post and $z/(w_{post}+ s) = 1$ is at the leading edge of the next consecutive post. It can be seen that all three curves in general have similar shapes; velocity increases from zero at the trailing edge of a post to a maximum near that edge and then decreases to a minimum near the leading edge of the next post and then increases again before it deceases to zero velocity at the leading edge of the next post, and is zero over the entire post surface. As can also be seen, there is only a small difference (about 3%) between the maximum velocities at $AF$ = 0.6 and $AF$ = 0.75. However, there is a more substantial increase (about 40%) in the velocity for the case of $AF$ = 0.75 compared with the velocity for the case of $AF$ = 0.44. In general, the high air fraction scenarios result in much greater velocities at this plane. These velocities represent the slip velocities and they signify reduction of frictional resistance in the channel.

Since the flowing liquid exerts a drag or a shear force on the surface of the channel, the reduction of liquid-solid contact area also affects the amount of shear stress that is applied to the solid surface by the liquid. In light of the observations made in Fig. 6, the wall shear stress on micro-posts is higher for surfaces with high cavity fractions. To confirm this, the shear stress on the cylindrical plane which passes through the post-top faces ($\tau_w$) normalized by the classical no-slip value ($\tau_{ns}$) along a line passing through the mid-cavity and mid post-top faces is plotted in Fig. 7 (b) as a function of $z/(w_{post}+ s)$ at three different air fractions (0.44, 0.60, and 0.75) and same Reynolds number of 400. It can be seen from this figure that as the flow approaches the post, for each air fraction the shear stress increases sharply along the edge of the post and then it decreases almost parabolically to a minimum at the middle of

the post and rises again to a peak value at the trailing edge of the post after which it drops sharply again back to a zero value as the flow reaches the cavity region. The rapid jump in each graph is due to high velocity gradients present along the edges. For each scenario the sharp increase in the shear stress appears to be higher along the trailing edge than the leading edge of the post. In addition, the shear stress on the post trailing edge at $AF = 0.75$ is approximately three times as there exists at $AF = 0.44$. Only a slight difference exists between the shear stresses at the $AF = 0.6$ and $AF = 0.75$. Hence, it is clear that the increase in the shear stress is non-linear with respect to the air fraction and it becomes extremely significant at high values of $AF$. As explained previously, this occurs because the surface area of the post is decreased while the inertia of the fluid which moves past the surface remains unchanged. The noticed velocity gradient and shear stress at the edges has a direct impact on surface drag or frictional resistance. The frictional resistance could be reduced by decreasing the velocity gradient at the wall. Modification of post geometry as discussed above could help in reducing velocity gradients; however, there are other issues and factors that need to be considered, for instance, susceptibility to wetting and fabrication.

*D.Influence of Reynolds Number Re*

In order to analyze the effect of the Reynolds number on the overall frictional resistance reduction, simulations were performed over the flow regimes $400 \leq Re \leq 1200$. A very useful parameter to use in overall characterization of any superhydrophobic surface is the friction factor Reynolds number product $fRe$. It represents the aggregate frictional resistance of a surface, averaging the high shear regions above a post with the zero shear above the cavities. For laminar flow the Darcy factor, $f$, is calculated with $\left( f = \frac{2\Delta P D}{\rho u^2 L} \right)$, where $u$ is the average velocity $\left( u = \frac{4\dot{m}}{\rho \pi D^2} \right)$. Then, the Poiseuille number $Po$ is obtained as:

$$Po = f\,Re \tag{9}$$

According to the conventional theory, $Po$ should be constant with the value of 64 for fully developed laminar flow in a circular pipe. Fig. 8 provides a graph of $fRe$ as a function of Reynolds number $Re$ for different air fractions ($AF = 0.44$, 0.6, and 0.75), and the data confirm the existence of a $Re$ dependency. It can be seen that the $fRe$ behavior is similar for all three $AF$ and the difference between the various $AF$ values is small. In general, $fRe$ is a monotonically increasing function of the $Re$ number and does not appear to asymptote out for large values of $Re$. The predicted results agree favorably with the experimental data of [4], who studied recently the flow inside a superhydrophobic micro-tube. They explained that the increase in $Po$ is due to the transition from Cassie state to Wenzel state. This explanation can now be supported by examining the CFD solution shown in Fig. 9 plotted when the water reached the end of the micro-pipe. Fig. 9 shows water volume fraction contours for the case of 0.6 air fraction at different Reynolds numbers on a 22.5º-plane passing through the square posts all the way till the end of the micro-pipe. It is obvious that as Reynolds number increases, the length of the micro-features region that becomes completely wetted with water increases (Fig. 9). Therefore, at high Reynolds number, the posts in-between cavities which are supposed to be filled with air to reduce skin-friction drag are no longer filled with water leading to high energy dissipation and, consequently, more drop in the total pressure (more drag). This indicates that the frictional performance of micro-pipes with square micro-posts features exhibits a Reynolds number dependence.

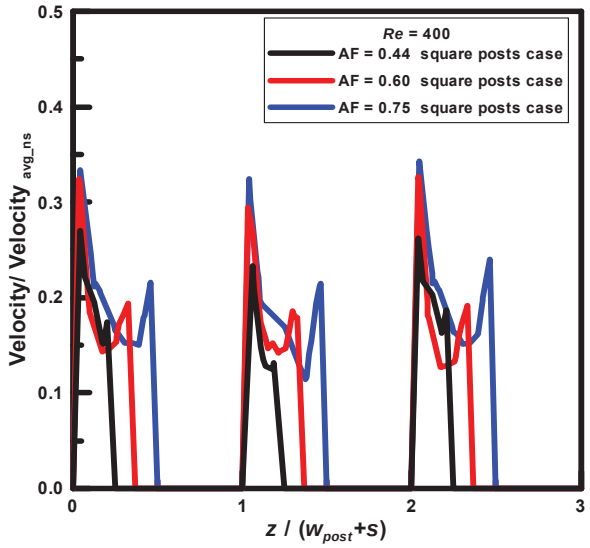


(a)

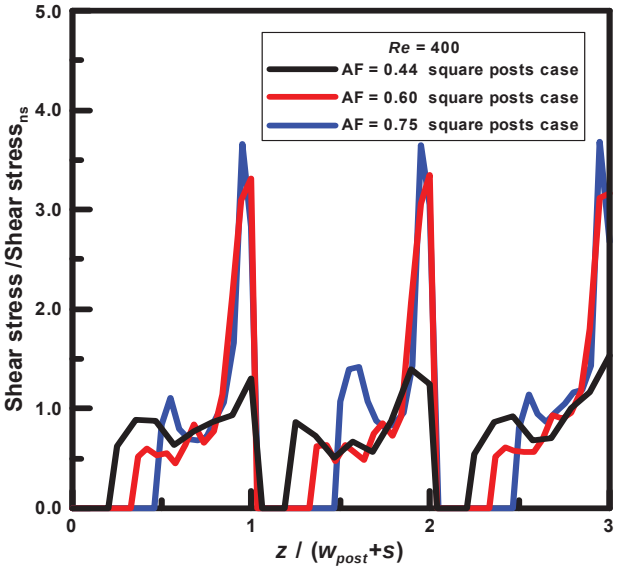


(b)

Fig. 7 (a) Normalized velocity distributions along a line passing over posts' faces at different air fractions and (b) Corresponding shear stress distributions

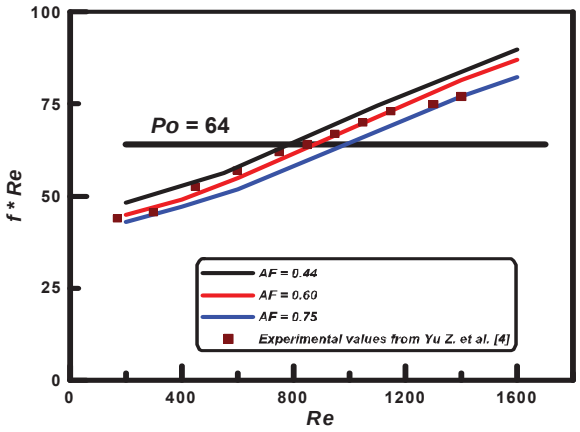


Fig. 8 Effect of Reynolds number on the Poiseuille number *Po* under different air fractions for superhydruphobic micro pipes patterned with micro-posts features

## IV. Conclusions

In this paper, numerical simulations of laminar fluid flows in superhydrophobic micro-pipes patterned with square micro-posts are presented. A VOF-based methodology has been adopted to visualize the dynamics of the flow characteristics inside the micro-pipes. Results of the present simulations revealed that, for superhydrophobic micro-pipes with micro-posts features, there is a strong dependency of the frictional resistance reduction on both air fractions and Reynolds number (*Re*). This reduction becomes increasingly more significant at large air fractions. Conversely, increasing *Re* reduces the frictional performance enhancement and, above certain *Re*, the increase of *Re* has an adverse effect on the frictional resistance reduction.

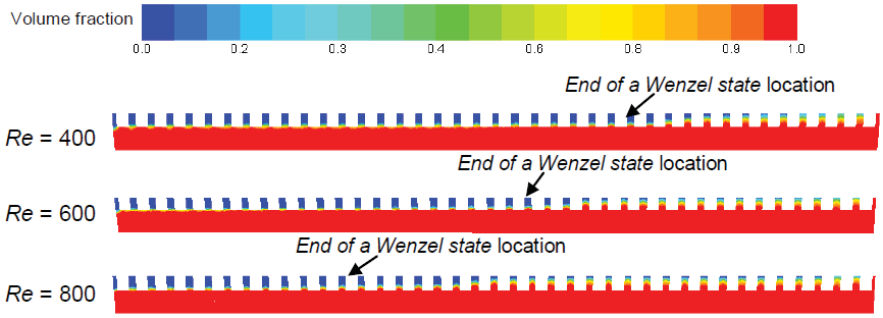


Fig. 9 Contour of water volume fractions at different Reynolds numbers for superhydrophobic micro-pipes having square posts features. (*AF* = 0.6)

## Acknowledgment

This work is supported and funded by the Public Authority of Education and Training under research project no. (TS-14-13). The project title is Numerical Study of Drag Reduction and Flow Enhancement over Superhydrophobic Surfaces.

## References

[1] Gad-El-Hak, M., 2007, "Flow Control: Passive, Active, and Reactive Flow Management," Cambridge University Press, Cambridge, UK, Chap. 10, pp. 205-228.
[2] Ou J., Perot B., and Rothstein J. P., 2004, "Laminar Drag Reduction in Microchannels Using Ultrahydrophobic Surfaces," Physics of Fluids, Vol. 16, no. 12, pp. 4635-4643.
[3] Guan N., Liu Z., Jiang G., Zhang C., and Ding N., 2015, "Experimental and Theoretical Investigations on the Flow Resistance Reduction and Slip Flow in Super-Hydrophobic Micro-Tubes," Experimental Thermal and Fluid Science, Vol. 69, pp. 45–57.
[4] Yu Z., Liu X., and Kuang G., 2015, "Water Slip Flows in Superhydrophobic Micro-Tubes with Laminar Flow Region," Chinese Journal of Chemical Engineering, Vol. 23, issue 5, pp. 763–768.
[5] Philip J., 1972, "Flows Satisfying Mixed No-Slip and No-Shear Conditions," Z. Angew. Math. Phys., Vol. 23, pp. 353-372.
[6] Lauga E. and Stone H.A., 2003, "Effective Slip in Pressure-Driven Stokes Flow," Journal of Fluid Mechanics, Vol. 489, pp. 55–77.
[7] Maynes D, Jeffs K, Woolford B, and Webb B., 2007, "Laminar Flow in a Micro-channel with Hydrophobic Surface Patterned Micro-Ribs Oriented Parallel to the Flow Direction," Physics of Fluids, Vol. 19, issue 9, 3603.
[8] Ng CO and Wang CY, 2011, "Effective Slip for Stokes Flow over a Surface Patterned with Two- or Three-Dimensional Protrusions," Fluid Dynamics Research, Vol. 43, no. 6, 065504.
[9] Ybert C, Barentin C, Cottin-Bizonne C, Joseph P, and Bocquet L., 2007, "Achieving Large Slip with Superhydrophobic Surfaces: Scaling Laws for Generic Geometries," Physics of Fluids, Vol. 19, issue 12, 3601.
[10] Gao P. and Feng J. J., 2009, "Enhanced Slip on a Patterned Substrate Due to Depinning of Contact Line," Physics of Fluids, Vol. 21, 102102.
[11] Park, H. W., 2015, "A Numerical Study of the Effects of Superhydrophobic Surfaces on Skin-Friction Drag Reduction in Wall-Bounded Shear Flows," Ph.D. Thesis, University of California, USA.
[12] Park, H. W., Park, H., and Kim J., 2013, "A Numerical Study of the Effects of Superhydrophobic Surface on Skin Friction Drag in Turbulent Channel Flow," Physics of Fluids, Vol. 25, 110815.
[13] Teo C. J. and Khoo B. C., 2014, "Effects of Interface Curvature on Poiseuille Flow through Microchannels and Microtubes Containing Superhydrophobic Surfaces with Transverse Grooves and Ribs," Microfluid Nanofluid, Vol. 17, pp. 891–905.
[14] Eleshaky, M.E., 2016, "Three-Dimensional VOF Simulations of Laminar Fluid Flows in Micro-Pipes Containing Superhydrophobic Walls with Micro-posts and Micro-Ridges," Proceedings of the ASME 2016 14th International Conference on Nanochannels, Microchannels, and Minichannels, submitted for publication.
[15] Hirt, C.W. and Nichols, B.D., 1981, "Volume of Fluid (VOF) Method for the Dynamics of Free Boundaries," Journal of Computational Physics, 39 (1), pp. 201–225.
[16] Brackbill J. U., Kothe D. B., and Zemach A., 1992, "A Continuum Method for Modeling Surface Tension," J. Comp. Phys., Vol. 100, pp. 335-354.
[17] FLUENT 13.1 User's Guide, Fluent Inc., 2010.

[18] Ubbink O., 1997, "Numerical Prediction of Two Fluid Systems with Sharp Interfaces," Ph. D. Thesis, Imperial College, University of London, UK.
[19] Lu S., Yao Z.H., Hao P.F., and Fu C.S., 2010, "Drag Reduction in Ultrahydrophobic Channels with Micro-Nano Structured Surfaces," Sci. China, Vol. 53, no. 7, pp. 1298–1305.